Characterization and Reactivity of Niobia Supported Copper Oxide Catalysts

Komandur V. R. Chary,* Kothapalli Kalyana Seela, Guggilla Vidya Sagar, and Bojja Sreedhar

Catalysis Division, Indian Institute of Chemical Technology, Hyderabad-500 007, India

Received: June 19, 2003; In Final Form: October 21, 2003

A series of niobia supported copper catalysts with varying copper loadings (1−15 wt %) were prepared by incipient wet impregnation method. The catalysts were characterized by X-ray diffraction (XRD), temperature-programmed reduction (TPR), UV−vis diffused reflectance spectra (UV-DRS), electron spin resonance (ESR), and X-ray photoelectron spectroscopy. Copper dispersion and metal area were determined by N_2O decomposition by passivation method. X-ray diffraction patterns indicate the presence of crystalline CuO phase above 2.5 wt % Cu on niobia. XPS peaks intensity ratio of Cu $2p_{3/2}$ to Nb $3d_{5/2}$ were compared with the Cu dispersion calculated from N_2O decomposition. ESR results suggest the presence of two types of copper species on niobia. TPR patterns reveal the presence of highly dispersed copper oxide at lower temperatures and bulk CuO at higher temperatures. The catalytic properties were evaluated for the vapor-phase dehydrogenation of cyclohexanol to cyclohexanone and related to copper dispersion.

Introduction

Copper based catalysts are of immense industrial importance such as in the reduction of nitric oxide,[1] synthesis of methanol,[2] steam reforming of methanol,[3] CO oxidation,[4] hydrogenolysis of esters,[5] CO hydrogenation,[6] and also in the dehydrogenation of cyclohexanol to cyclohexanone.[7−9] In many instances, the active CuO is supported on oxides such as Al_2O_3, SiO_2, ZrO_2, and TiO_2 in combination with Zn or other transition metals such as Ru and Fe. The catalytic properties of the active copper phase can be greatly influenced by the nature of supported oxide and dispersion of the active component.[10] However, the nature of active species of these catalysts is still the subject of extensive investigation by many researchers.

Niobium compounds and the niobium-containing materials are very useful as catalysts, catalyst supports, or promoters in various reactions of industrial importance.[11−13] Among the properties that determined the interest for these materials, a few are very important for catalysis: their acidic and redox properties and also the catalyst life extension obtained when a small amount of niobium oxide is added to known catalysts.[11−16] Niobia was one of the supports examined to prove the reducibility of the support, which is a key factor in the development of SMSI for metal catalysts subjected to a high-temperature reduction.[17] There are several reports on the same effect using Pt, Ni, Rh, and Co as active metals.[18−21] The catalytic properties observed in the structure-sensitive reactions such as the hydrogenolysis of hydrocarbons are strongly suppressed by SMSI, but this suppression is moderate in structure-sensitive reactions such as dehydrogenation of hydrocarbons.[22] However, Parvulescu et al.[21] found that the activity-determinating factor in hydrogenolysis is not the SMSI but the effect of the crystallite size or the presence of toxins from the metal precursor, such as Cl^- from $NbCl_5$. Hence, the characterization of the niobium compounds is very important to the discussion of their catalytic activity and for the prediction of both their activity and selectivity in various reactions.

Catalytic dehydrogenation of cyclohexanol to cyclohexanone is an industrially important reaction in the production of caprolactum. Copper based catalysts are used in the dehydrogenation of cyclohexanol,[23] which is produced either by hydrogenation of phenol or by air oxidation of cyclohexane. The catalytic dehydrogenation of cyclohexanol has gained much importance.[7,8] Sideitseva and Erofeev[24] have studied the dependence of the metal deposition procedure on the specific surface and catalytic properties of Cu/MgO catalysts. Petrova et al.[25] have examined the promotional role of cadmium in Cu/Al_2O_3 alloy catalysts. Copper based catalysts have been studied in the dehydrogenation[26] and oxidative dehydrogenation[27] of cyclohexanol in which cyclohexene is one of the byproducts of the reaction.[26−28]

The study of determination of the dispersion of the active phase in supported Cu catalysts is an interesting topic of research in recent years for understanding the role of active phase on the catalytic properties. A fundamental understanding of the structure−activity relationships observed in heterogeneous catalytic dehydrogenation is of basic importance for the development of new catalytic materials and for improving the performance of existing catalysts. For this, N_2O decomposition was studied to find active phase dispersion in supported copper catalysts.[3]

In the present investigation, we report the use of niobia support for Cu catalysts. The catalysts were characterized by XRD, UV-DRS, ESR, TPR, XPS and Cu dispersion, metal area by N_2O decomposition. The catalytic properties were evaluated for the vapor phase dehydrogenation of cyclohexanol to cyclohexanone. The purpose of this work is to estimate the dispersion of CuO supported on niobia as a function of copper loading and to identify changes in the structure of the CuO phase with loading and also to understand the relation between the dispersion of Cu and the activity/selectivity during dehydrogenation of cyclohexanol.

Experimental Section

Niobium (V) oxide was prepared by calcination of niobium pentoxide hydrate (Niobia, HY-340, AD/1227, CBMM, Brazil)

* Corresponding author. Fax: +91-40-27160921; e-mail: kvrchary@iict.res.in.

10.1021/jp035738s CCC: $27.50
Published on Web 12/12/2003

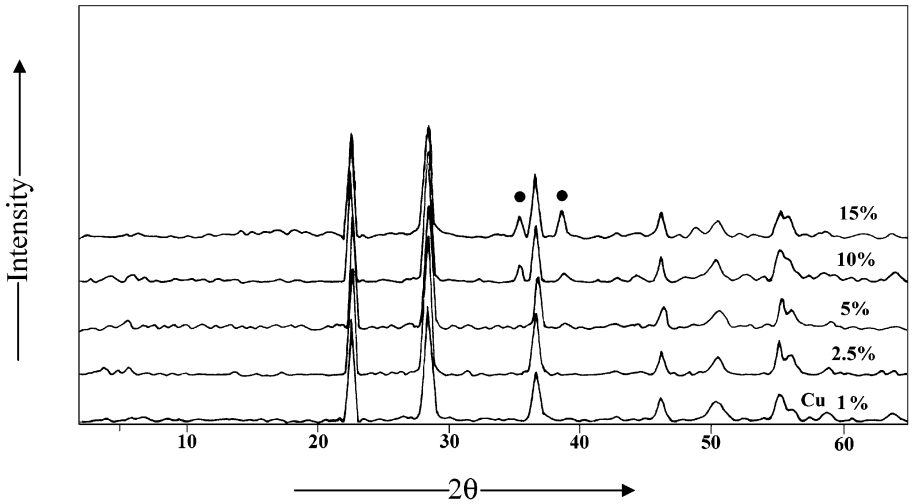

Figure 1. X-ray diffractogramms of $CuO-Nb_2O_5$ catalysts (●-reflections because of CuO).

in air at 773 K for 5 h to yield Nb_2O_5 (BET specific surface area 55 m^2/g). A series of copper catalysts with Cu loadings varying from 1 to 15% w/w were prepared by wet impregnation of $Cu(NO_3)_2 \cdot 3H_2O$ (Fluka) on the Nb_2O_5 support. The samples were dried at 383 K for 16 h and subsequently calcined at 773 K for 5 h in air.

X-ray diffractograms were recorded on a Seimens D 5000 diffractometer using graphite filtered CuKα radiation at 40 kV and 30 mA. XRD patterns were obtained in the region from 0 to 65° with a scan speed of 6° min^{-1}.

The UV−vis diffused reflectance spectra were recorded on a GBC UV−visible Cintra 10_e spectrometer with an integrating sphere reflectance accessory. The spectra were recorded in air at room temperature and the data was transformed according to the Kubelka−Munk equation $f(R) = (1-R_\alpha)\ 2/2r_\alpha$.

ESR spectra of the precalcined samples were recorded on a Bruker EMX-X band spectrometer at the X-band frequency 9.7667 GHz at 293 K. The spectra were calibrated with ER 035M NMR Gauss meter.

The X-ray photoelectron spectroscopy (XPS) spectra of catalysts was measured on an XPS spectrometer (Kratos-Axis 165) with Mg Kα radiation (1253.6 eV) at 75 W. The C1s line at 284.6 eV was used as an internal standard for the correction of binding energies. The background pressure during the data acquisition was kept below 10^{-10} bar.

Temperature-programmed reduction studies were conducted on AutoChem 2910 (Micromeritics) instrument. In TPR experiment, 100 mg of oven-dried sample (dried at 373 K for 15 h) was taken in a U-shaped quartz sample tube. The catalyst was mounted on a quartz wool plug. Prior to TPR studies, the catalyst sample was pretreated by passing helium gas in a flow of 50 mL/min at 393 K for 2 h. After pretreatment, the sample was cooled to ambient temperature and TPR analysis was carried out in a flow of 5% H_2-Ar (50 mL/min) from ambient temperature to 723 K at a heating rate of 10 K/min. H_2 consumption and T_{max} positions are calculated using GRAMS/32 software.

Copper surface area and percentage dispersion were calculated by N_2O decomposition conducted on AutoChem 2910 (Micromeritics). This method was based on the decomposition of N_2O over metallic surface, which releases N_2.[29] The catalysts were pretreated in helium flow (50 mL/min) and heated at 393 K for 30 min. The catalysts were reduced with a flow mixture of 5% H_2-Ar raising the temperature at a heating rate of 10 K/min up to 723 K. In sequence, oxidation with N_2O was performed at 333 K for 1 h flowing N_2O (50 mL/min). Reduction of the surface oxide sublayer was performed similarly as in TPR raising the temperature to 723 K.

A down flow fixed bed reactor operating at atmospheric pressure and made of Pyrex glass was used to test the catalysts during the dehydrogenation of cyclohexanol to cyclohexanone. About 500 mg of the catalyst diluted with an equal amount of quartz grains was charged into the reactor and was supported on a glass wool bed. Prior to introducing the reactant cyclohexanol with a syringe pump, the catalyst was reduced at 573 K for 3 h, in purified hydrogen flow. After the prereduction, the reactor was fed with cyclohexanol in N_2 (flow rate 50 mL/min), which is used as carrier gas. The liquid products, mainly cyclohexanone and cyclohexene, were analyzed by a Hewlett-Packard 6890 gas chromatograph equipped with a flame ionization detector using HP-5 capillary column. The products were also identified using HP 5973 quadruple GC-MSD system using HP-1MS capillary column.

Results and Discussion

The X-ray diffraction patterns of CuO catalysts supported on Nb_2O_5 calcined at 773 K are shown in Figure 1. In all the samples, XRD peaks due to low-temperature niobia were observed at $d = 3.95$, 3.14, 2.45, 1.97, and 1.66 Å. Ko and Weissman[30] reported that, at low calcination temperature (<773 K), the samples are X-ray amorphous. However, the samples calcined between 773 and 873 K show the TT-phase of Nb_2O_5, and the samples calcined between 873 and 973 K favor the formation of T-phase of Nb_2O_5. At 1073 K of calcination, M-phase, and at 1273 K and above, H-phase, of Nb_2O_5 is observed. In the present study, the samples were calcined at 773 K and our XRD results (Figure 1) also suggest the formation of TT-phase of Nb_2O_5, which is in good agreement with the work of Ko and Weissman.[30] At the low Cu loadings, the diffractogramms did not indicate the presence of characteristic peaks due to crystalline CuO phase along with very intense peaks due to Nb_2O_5 (TT-phase). The most intense XRD line due to CuO, corresponding to (111) plane at $d = 2.52$ Å, was observed only beyond 2.5% w/w of Cu loading on Nb_2O_5 (shown with closed circles in Figure 1). The intensity of this peak increases with the increase of Cu loading in the catalysts. The XRD patterns also indicate that no characteristic peaks were found because of the formation of a mixed oxide phase between CuO and Nb_2O_5 even at the highest Cu loading of this investigation. The absence of XRD peaks due to CuO at lower

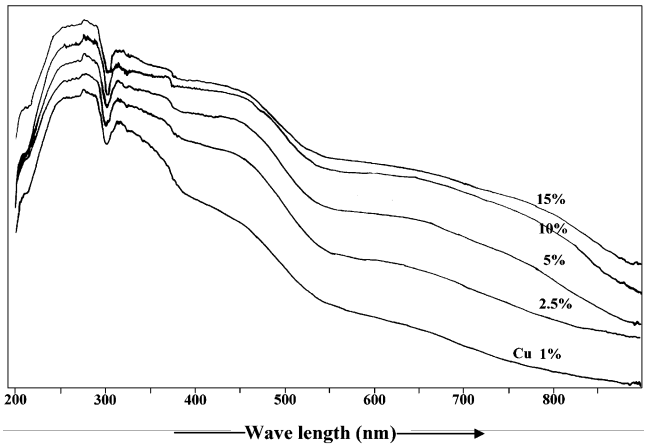

Figure 2. UV-DR spectra of $CuO-Nb_2O_5$ catalysts.

loadings indicate that the CuO phase is present in a highly dispersed amorphous state on the support. The size of CuO crystallites might be less than 40 Å, which is beyond the detection capacity of the powder XRD technique.

The UV-DR spectra of calcined samples are shown in Figure 2. The catalysts show very similar DR spectra, with a strong absorption band at 270 nm and a large absorption band at ~650 nm. According to previous results,[31,32] the band at 270 nm can be attributed to the charge transfer between surface oxygen and isolated Cu^{2+} ions while the large absorption band at ~650 nm is associated with the $^2E_g \Longrightarrow {}^2T_{2g}$ process, the spin allowed transition of the Cu^{2+} ions in the distorted octahedral sites of cubic CuO phase. By increasing the copper content, the c.t. band of copper ions becomes broader, showing an additional shoulder at 350 nm, indicating the formation of small amount of copper clusters in a highly dispersed state, not detectable by XRD. According to an earlier report,[31] a band around 700 nm and a stronger absorption band between 250 and 290 nm characterized for copper−alumina samples. Shimokawabe et al.[33] have observed that the broadening of the charge transfer transition band and a shoulder at 350 nm indicate the formation of a small amount of copper clusters in a highly dispersed state. The intensity of the peak at 650 nm increased with Cu loading which clearly indicates the increase of crystalline and bulk CuO.

ESR spectra of calcined samples recorded at room temperature are shown in Figure 3. All the spectra can be interpreted in terms of the overlap of at least two ESR signals. The first one is an axial signal with a resolved hyperfine structure visible in the parallel region and typical of Cu^{2+} containing systems. The second signal is broad, unstructured, and slightly axial. The spectra actually observed are partially resolved in the parallel region only. The resolution decreases with increasing copper content. The spin Hamiltonian parameters for both the signals were evaluated and given in Table 1. The first signal can be attributed to isolated or nearly isolated copper ions in axial symmetry, probably an axially distorted octahedral environment, and its parameters are close to those previously reported for copper−alumina systems.[31,34] The second signal showing an unresolved hyperfine splitting could be attributed to the Cu^{2+} species interacting with each other and generally referred to as clustered Cu^{2+} ions. Table 1 reveals that there are two types of Cu^{2+} ions, which are chemically inequivalent. The anisotropic signal intensity decreased with an increase in Cu content. This may be due to the formation of aggregates, by spin pairing that occurs when the distance between the ions is too close resulting in dipolar broadening, which can be evidenced from UV-DRS and also by XRD. The Cu^{2+} hyperfine splitting observed in the catalyst (1 wt % Cu) reveals the isolated nature of copper ions.

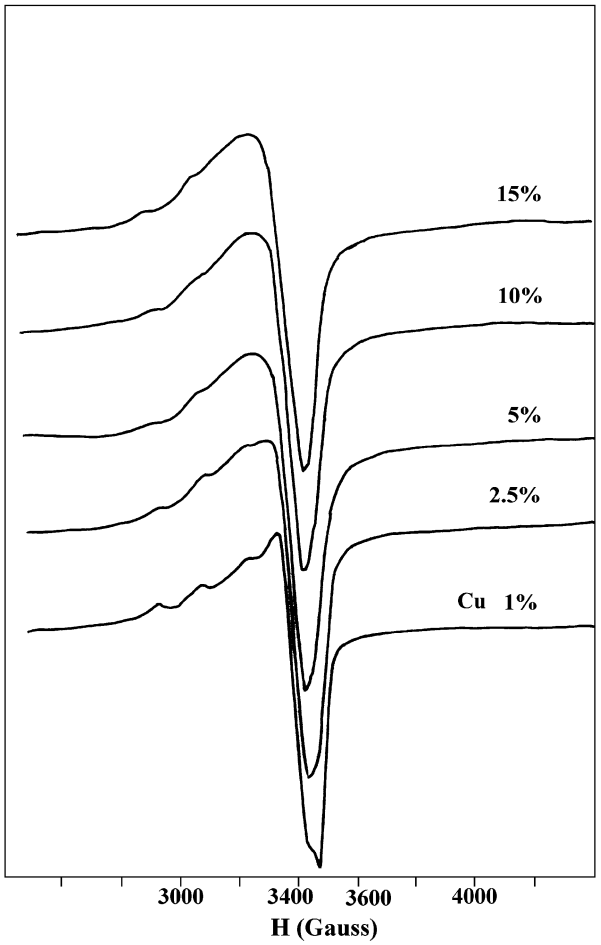

Figure 3. Electron spin resonance spectra of $CuO-Nb_2O_5$ catalysts.

TABLE 1: ESR Parameters of $CuO-Nb_2O_5$ Catalysts

S. No.	Cu wt %	$g^{\parallel}$	$A^{\parallel}$	$g^{\perp}$	$A^{\perp}$
1	1	2.23	135	2.03	76
2	2.5	2.21	127	2.03	76
3	5	2.22	172.5	2.04	105.3
4	10	2.21	175	2.04	101.3
5	15	2.21	154	2.04	145

The XPS spectra of Cu 2p and Nb 3d for various copper oxide catalysts supported on niobia with different copper loadings are shown in Figure 4 and Figure 5, respectively. The presence of shake up satellite peaks on the spectra suggests the copper oxidation state as +2. The lowering of binding energy in the present study may occur because of the X-ray and ion bombardment induced reduction of Cu^{2+} state.[35] The Nb 3d binding energy values are in the range of 207.5 eV. The binding energy of 207.5 eV is well fit with the corresponding binding energy of niobia.[36] It is very clear from the Table 2 that the niobium is present in a single oxidation state of 5+ in all the catalysts studied indicating that Nb_2O_5 structure was not modified with the copper impregnation. Table 2 presents the exact binding energy values of Cu $2p_{3/2}$, Nb $3d_{5/2}$, and their FWHM values.

Figure 6 shows the relation between the copper loading on niobia and XPS intensity ratio (Cu 2p/Nb 3d). The XPS intensity ratio was found to increase with increasing Cu loading up to 5 wt % (Table 2) and did not change appreciably with further increase in the Cu loading. This might be due to the formation of crystalline CuO at higher loadings, which can be evidenced from XRD results. Thus, a low dispersion of copper oxide is

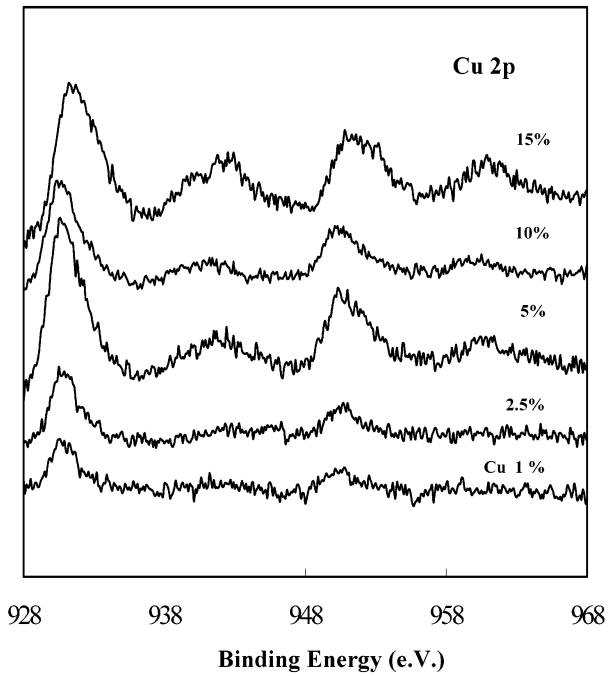

Figure 4. X-ray photoelectron spectra of Cu 2p spectra of various $CuO-Nb_2O_5$ catalysts.

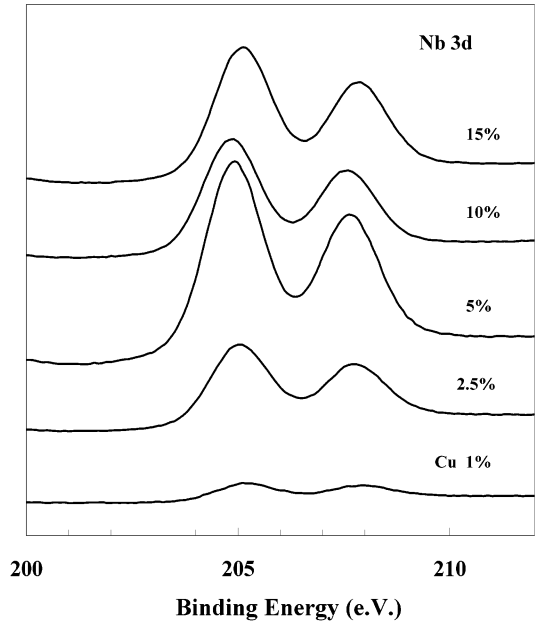

Figure 5. X-ray photoelectron spectra of Nb 3d spectra of various $CuO-Nb_2O_5$ catalysts.

TABLE 2: ESCA Results of $CuO-Nb_2O_5$ Catalysts

S. No.	Cu wt %	position and FWHM of $Cu2p_{3/2}$	position and FWHM of $Nb3d_{5/2}$	XPS intensity I_{Cu}/I_{Nb}
1	1	932.9 (1.702)	207.2 (1.48)	0.092
2	2.5	932.9 (1.876)	207.05 (1.511)	0.22
3	5	932.9 (2.13)	206.9 (1.5)	0.35
4	10	932.8 (1.96)	206.8 (1.45)	0.34
5	15	933.6 (2.54)	207.1 (1.48)	0.35

noticed at higher loadings by N_2O decomposition method described later in this section. Thus, the present XPS results are in well agreement with the dispersion of copper determined by N_2O decomposition method.

The reducibility of copper species in $Cu-Nb_2O_5$ catalysts was investigated by TPR experiments and the profiles are given

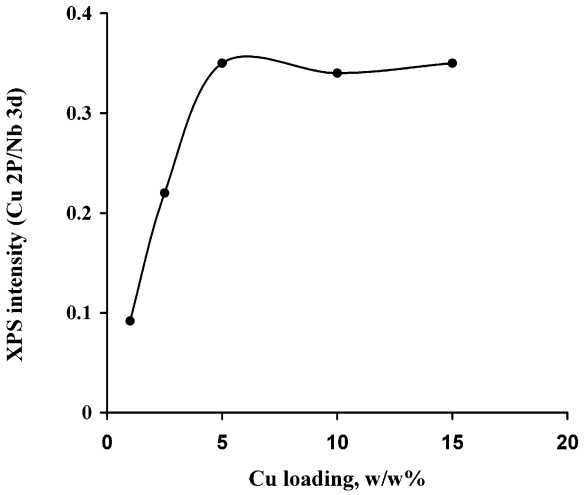

Figure 6. Relation between Cu loading to XPS intensity (Cu2p/Nb3d).

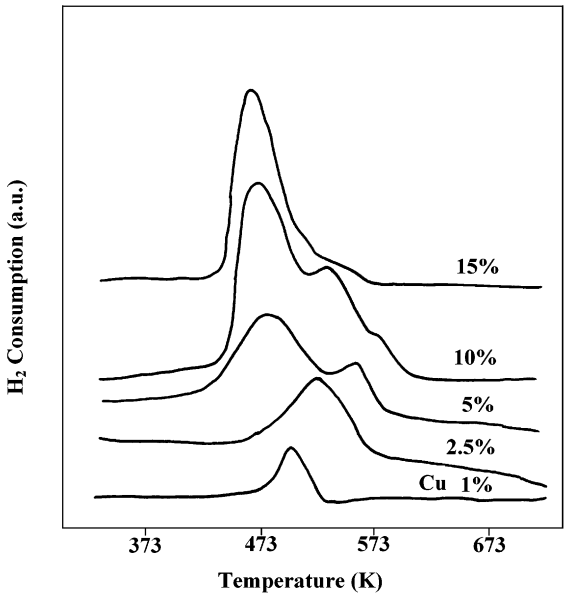

Figure 7. Temperature-programmed reduction profiles of $CuO-Nb_2O_5$ catalysts.

in Figure 7. All the samples exhibit two reduction profiles during TPR in the temperature range of 473−573 K except for the sample with 1 and 2.5% loading. Yan et al.[37] reported similar observations in their study of deactivation of Cu-ZSM-5 zeolite catalysts for the selective catalytic reduction of NO and also compared the reduction of copper on various supports. It was reported that the surface copper oxide species on the support is more easily reduced than the bulk CuO.[38−43] The T_{max} position of first peak is shifting to low-temperature region with the increase of Cu loading. When the copper loading is above 2.5%, a second reduction peak at 493 K is observed (Figure 7). For the 5 wt % $Cu-Nb_2O_5$ catalyst, the TPR peak at a low-temperature region is attributed to the highly dispersed surface CuO species, and the TPR peak observed at a high-temperature region is attributed to the bulk CuO. The reduction peak is shifted toward high temperatures and peaks become relatively broad with increasing Cu content. The broadening of the peak and the shifting of the T_{max} toward high temperatures may be due to the increase in crystallininty of CuO with increase in Cu loading as evidenced from XRD results. Hydrogen consumption values and T_{max} during the TPR are given in Table 3; it is observed that the H_2 consumption of the first peak is maximum

TABLE 3: Temperature-Programmed Reduction Results of Various $CuO-Nb_2O_5$ Catalysts

S. No.	Cu wt %	T_{max}^1 (K)	H_2 consumption^1 μ mol/g	T_{max}^2 (K)	H_2 consumption^2 μ mol/g
1	1	545	155		
2	2.5	523	375		
3	5	489	148	566	585
4	10	518	123	576	1450
5	15	517	113	580	2301

TABLE 4: Dispersion, Copper Metal Area, and Activity Results of $CuO-Nb_2O_5$ Catalysts

S. No.	Cu wt %	Cu metal area m^2/g_{Cu}	% dispersion	% conversion	% selectivity of c-hexanone	% selectivity of c-hexene	TOF sec^{-1}
1	1	75.3	11.7	12	6.5	93.5	0.82
2	2.5	140.5	21.8	24	65	35	0.34
3	5	79.8	12.4	19	68	32	0.22
4	10	40.6	6.3	22	72	28	0.3
5	15	24.3	3.8	19	62	38	0.2

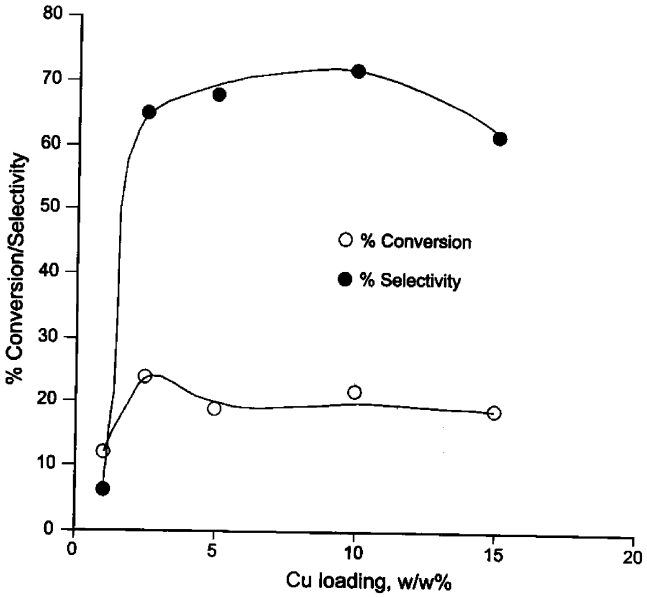

Figure 8. Dehydrogenation of cyclohexanol on $CuO-Nb_2O_5$ catalysts (reaction temperature 523 K, GHSV 6720 h^{-1}).

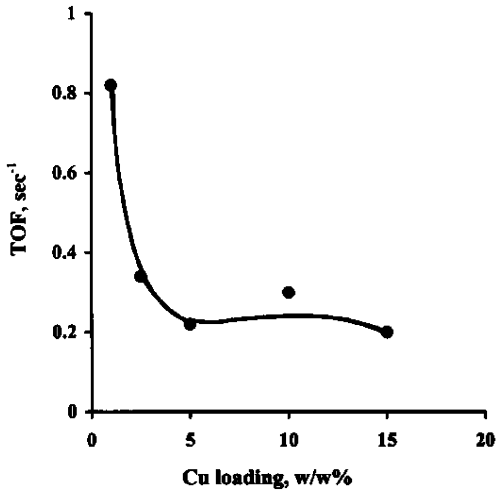

Figure 9. Relationship between copper loading vs TOF.

for 2.5 wt % of Cu. This clearly shows that the dispersion is high for 2.5 wt % and decreases with further copper loading.

The dispersion values given in Table 4 are those calculated from N_2O uptake data using the following equation:

$$N_2O_{(gas)} + 2\,Cu_{(s)} \rightarrow Cu_{(s)}-O-Cu_{(s)} + N_{2(gas)}$$

The copper metal areas were determined using the equation $S_H = n_m^s X_m n_s^{-1}$, where S_H is the total metallic surface area, n_m^s is the total nitrous oxide molecules decomposed, X_m is the chemisorption stoichiometry at monolayer coverage, and n_s^{-1} is the number of copper metal atoms per unit area of surface (1.47×10^{19} m^{-2}). Table 4 gives the values of percentage dispersion and Cu metal areas (m^2/g Cu), and it was observed that the dispersion and metal areas are the highest for 2.5 wt % of Cu on Nb_2O_5. On further increase in the copper loading, the dispersion and metal areas are decreased.

The catalytic properties during the vapor phase dehydrogenation of cyclohexanol exhibited by various CuO/Nb_2O_5 catalysts are shown in Figure 8. As can be seen from Figure 8, the cyclohexanol activity increases with increase in Cu loading up to 2.5 wt %. There is not much change in the activity observed with further increase in the Cu loading on niobia. The conversion for 1 wt % Cu loading catalyst was 12% and increases to 24% as the copper loading increased to 2.5%. The selectivity toward cyclohexanone was very less for 1 wt % catalyst. However, further increase in copper loading on niobia has increased the selectivity drastically toward cyclohexanone to 65% from 6.5%. The selectivity was increased with further increase in the copper loading except a slight decrease is observed for 15 wt % catalyst. This may be due to increase in crystallinity which makes more support surface available for dehydration activity at 523 K which can be evidenced from XRD and ESR. Cyclohexene was observed as the only byproduct. To find out the relation between the dehydrogenation of cyclohexanol and the copper loading, a plot of copper loading on niobia versus TOF is shown in Figure 9, wherein the TOF is equal to the rate of cyclohexanol molecules converted per second per site of copper. TOF is constant for all the catalysts except for the Cu 1 wt % catalyst. This may be due to the isolated copper ions present in the 1 wt % catalyst, which can be clearly evidenced from the ESR results.

Conclusions

XRD results reveal the presence of crystalline CuO at higher copper loadings (>2.5%). N_2O decomposition is a better method for measuring the dispersion of Cu on niobia. Copper oxide disperses well on niobium oxide. The dispersion of copper oxide on the surface of niobia increased to 2.5% and decreased further at higher loadings. The information obtained by UV-DR spectra, ESR, and TPR reveal the presence of two types of copper species on the niobia support. The dispersion of Cu determined by N_2O decomposition substantiates the findings of XPS and XRD. CuO supported on niobia are highly active for the vapor phase dehydrogenation of cyclohexanol. The catalytic activity during the dehydrogenation of cyclohexanol is directly correlated to the dispersion of copper.

Acknowledgment. The authors are grateful to CBMM, Brazil, for providing a hydrated niobia sample. The authors K.K.S. and G.V.S. thank CSIR for the award of senior research fellowship.

References and Notes

(1) Kim, T.-W.; Song, M.-W.; Koh, H.-L.; Kim, K.-L. *Appl. Catal., A* **2001**, *210*, 35.
(2) Weigel, J.; Frohlich, C.; Baiker, A.; Wokaun, A. *Appl. Catal., A* **1996**, *140*, 29.
(3) Velu, S.; Suzuki, K.; Okazaki, M.; Kapoor, M. P.; Osaki, T.; Ohashi, F. *J. Catal.* **2000**, *194*, 373.
(4) Martinez-Arias, A.; Fernandez-Garcia, M.; Galvez, O.; Coronado, J. M.; Anderson, J. A.; Conesa, J. C.; Soria, J.; Munuera, G. *J. Catal.* **2000**, *195*, 207.
(5) Brands, D. S.; Poels, E. K.; Bliek, A. *Appl. Catal., A* **1999**, *184*, 279.
(6) Tavares Figueiredo, R.; Martinez-Arias, A.; Lopez Granados, M.; Fierro, J. L. G. *J. Catal.* **1998**, *178*, 146.
(7) Fabina, M. T.; Schmal, M.; Schmal, M. *Appl. Catal., A* **1997**, *163*, 153.
(8) Fridman, V. Z.; Davydov, A. A. *J. Catal.* **2000**, *195*, 20.
(9) Chang, H. F.; Slague M. A. *J. Mol. Catal.* **1994**, *88*, 223.
(10) Dandekar, A.; Vannice, M. A. *J. Catal.* **1998**, *178*, 621.
(11) Tanabe, K. *Catal. Today* **1990**, *8*, 1.
(12) Tanabe, K. *Chem. Technol.* **1991**, *21*, 628.
(13) Tanabe, K.; Okazaki, S. *Appl. Catal., A* **1995**, *133*, 191.
(14) Carniti, P.; Gervasini, A.; Auroux, A. *J. Catal.* **1994**, *150*, 274.
(15) Batamack, P.; Vincent, R.; Fraissard, J. *Catal. Lett.* **1996**, *36*, 81.
(16) Vedrine, J. C.; Coudurier, G.; Ouqour, A.; de Oliveira, P. G. P.; Volta, J. C. *Catal. Today* **1996**, *28*, 3.
(17) Tauster, S. J.; Fung, S. C. *J. Catal.* **1978**, *55*, 29.
(18) Passos, F. B.; Aranda, D. A.; Soares, R. R.; Schmal, M. *Catal. Today* **1998**, *43*, 3.
(19) Kunimori, K.; Oyanagi, H.; Shindo, H. *Catal. Lett.* **1993**, *21*, 283.
(20) Kunimori, K.; Hu, Z.; Uchijima, T.; Asakura, K.; Iwasawa, Y.; Soma, M. *Catal. Today* **1990**, *8*, 85.
(21) Parvulescu, V.; Ruwet, M.; Grange, P.; Parvulescu, V. I. V. *J. Mol. Catal.* **1998**, *135*, 75.
(22) Uchijima, T. *Catal. Today* **1996**, *28*, 105.
(23) Pearse, R.; Patterson, W. R. *Catalysis and Chemical Processes*; Leonard Hill: Glasgow, 1981; p 274.
(24) Sideitseva, M. A.; Erofeev, B. V. *Bul. Acad., Sci. USSR, Div. Chem. Soc.* **1986**, *2*, 30.
(25) Petrova, V.; Orizavski, I.; Draganov, A. *Khim. Imd. (Sofia)* **1983**, *9*, 401.
(26) Dobrovolszky, M.; Tetenyi, P.; Paal, A. *J. Catal.* **1982**, *74*, 31.
(27) Yu Ming Lin; Ikai Wang; Chium Tih Yeh *Appl. Catal.* **1988**, *41*, 53.
(28) Uemichi, Y.; Sakai, T.; Kanzuka, T. *Chem. Lett.* **1989**, 777.
(29) Bond, G. C.; Namijo, S. N. *J. Catal.* **1989**, *118*, 507.
(30) Ko, E. I.; Weissman, J. G. *Catal. Today* **1990**, *8*, 27.
(31) Centi, G.; Perathoner, S.; Billing, D.; Giamello, E. *J. Catal.* **1995**, *151*, 75.
(32) Marion, M. C.; Garboeski, E.; Primet, M. *J. Chem. Soc., Faraday Trans.* **1990**, *86*, 3027.
(33) Shimokawabe, M.; Asakawa, H.; Takezawa, N. *Appl. Catal.* **1990**, *59*, 45.
(34) Dow, W.; Wang, Y.; Huang, T. *J. Catal.* **1996**, *160*, 155.
(35) Chusuei, C. C.; Brooksheir, M. A.; Goodman, P. W. *Langmuir* **1999**, *15*, 2806.
(36) Moulder, J. F.; Stickle, W. F.; Sobol, P. E.; Bomben, K. D. *Handbook of XPS*; Perkin-Elmer Corporation: Eden Prairie, MN, 1992.
(37) Yan, J. Y.; Lei, G. D.; Sachtler, W. M. H.; Kung, H. H. *J. Catal.* **1996**, *161*, 43.
(38) Fierro, G.; Lojacono, M.; Inversi, M.; Porta, P.; Lavecihia, R.; Cioci, F. *J. Catal.* **1994**, *148*, 709.
(39) Zhou, R.; Yu, T.; Jiang, X.; Chen, F.; Zheng, X. *Appl. Surf. Sci.* **1999**, *148*, 263.
(40) Shimokabe, M.; Asakawa, H.; Takezawa, N. *Appl. Catal.* **1990**, *59*, 45.
(41) Robertson, S. D.; Minicol, B. D.; Debaos, J. H.; Kloet, S. C.; Jenkins, J. W. *J. Catal.* **1975**, *37*, 424.
(42) Vander Grift, C. J. G.; Mulder, A.; Geus, J. W. *Appl. Catal.* **1990**, *60*, 181.
(43) Delk, F. S.; Vavere, A. *J. Catal.* **1994**, *147*, 322.